

---

---

# In Vivo Kinetic and Steady-State Quantification of $^{18}\text{F}$ -CPFPX Binding to Rat Cerebral $A_1$ Adenosine Receptors: Validation by Displacement and Autoradiographic Experiments

David Elmenhorst<sup>1</sup>, Tina Kroll<sup>1</sup>, Franziska Wedekind<sup>1</sup>, Angela Weisshaupt<sup>1</sup>, Simone Beer<sup>1,2</sup>, and Andreas Bauer<sup>1,3</sup>

<sup>1</sup>Institute of Neuroscience and Medicine, INM-2, Forschungszentrum Jülich, Jülich, Germany; <sup>2</sup>Central Institute for Electronics, Forschungszentrum Jülich, Jülich, Germany; and <sup>3</sup>Neurological Department, Medical Faculty, Heinrich-Heine-University Düsseldorf, Düsseldorf, Germany

---

In vivo imaging of the  $A_1$  adenosine receptor ( $A_1$ AR) using  $^{18}\text{F}$ -8-cyclopentyl-3-(3-fluoropropyl)-1-propylxanthine ( $^{18}\text{F}$ -CPFPX) and PET has become an important tool for studying physiologic and pathologic states of the human brain. However, dedicated experimental settings for small-animal studies are still lacking. The aim of the present study was therefore to develop and evaluate suitable pharmacokinetic models for the quantification of the cerebral  $A_1$ AR in high-resolution PET. **Methods:** On a dedicated animal PET scanner, 15 rats underwent  $^{18}\text{F}$ -CPFPX PET scans of 120-min duration. In all animals, arterial blood samples were drawn and corrected for metabolites. The radioligand was injected either as a bolus or as a bolus plus constant infusion. For the definition of unspecific binding, the  $A_1$ AR selective antagonist 8-cyclopentyl-1,3-dipropylxanthine (DPCPX) was applied. After PET, the brains of 9 animals were dissected and in vitro saturation binding was performed using high-resolution  $^3\text{H}$ -DPCPX autoradiography. **Results:** The kinetics of  $^{18}\text{F}$ -CPFPX were well described by either compartmental or noncompartmental models based on arterial input function. The resulting distribution volume ratio correlated with a low bias toward identity with the binding potential derived from a reference region (olfactory bulb) approach. Furthermore, PET quantification correlated significantly with autoradiographic in vitro data. Blockade of the  $A_1$ AR with DPCPX identified specific binding of about 45% in the reference region olfactory bulb. **Conclusion:** The present study provides evidence that  $^{18}\text{F}$ -CPFPX PET based on a reference tissue approach can be performed quantitatively in rodents in selected applications. Specific binding in the reference region needs careful consideration for quantitative investigations.

**Key Words:** positron emission tomography; autoradiography; blocking experiment; kinetic modeling;  $^{18}\text{F}$ -CPFPX; adenosine  $A_1$  receptor

**J Nucl Med 2013; 54:1411–1419**

DOI: 10.2967/jnumed.112.115576

---

**T**he  $A_1$  adenosine receptor ( $A_1$ AR) is a G-protein–coupled receptor that modulates synaptic transmission and neuronal excitability (1). The  $A_1$ AR has been proposed to contribute to various

neurologic and psychiatric disorders (2), physiologic processes such as caffeine-induced neurostimulation, and sleep–wake regulation (3).

These observations created a high interest in imaging cerebral  $A_1$ AR activity. So far, 2  $A_1$ AR-specific radioligands have been applied in humans. PET with  $^{18}\text{F}$ -8-cyclopentyl-3-(3-fluoropropyl)-1-propylxanthine ( $^{18}\text{F}$ -CPFPX) and [1-methyl- $^{11}\text{C}$ ]8-dicyclopropylmethyl-1-methyl-3-propylxanthine has been used to visualize and quantify the  $A_1$ AR in vivo (4). Both compounds are xanthine-type antagonists of the  $A_1$ AR.

In previous reports we have described the quantification of  $^{18}\text{F}$ -CPFPX PET in humans using arterial input and a noninvasive reference region approach (5). Clinical applications and studies in neuroscience (4) proved the suitability and innovative potential of this new imaging method. Currently, numerous agonists, antagonists, and allosteric modulators are under development to explore the therapeutic potential of adenosine receptors (6). Experimental animal imaging could streamline the evaluation process of these compounds, and animal models of adenosine-related diseases might help to identify potential applications.

It is therefore important to test the suitability of quantitative  $^{18}\text{F}$ -CPFPX PET in a dedicated small-animal PET system. The purpose of the present study was to evaluate pharmacokinetic models in rats using both arterial input function and reference tissue methods. A special focus was put on noninvasive quantification because this approach will facilitate longitudinal studies allowing repeated investigations in identical animals.

Because of species differences in the cerebral distribution of  $A_1$ ARs, human quantification methods cannot be transferred to rats and mice without modification. Especially, the reference region in human studies (cerebellum) must not be applied in rodents, because the cerebellum is among the brain regions with the highest  $A_1$ AR densities in rodents. Instead, we evaluated the olfactory bulb as a reference region for brain PET studies in rats.

The suitability of both reference region and quantification methods was evaluated by in vivo binding and blocking experiments. The results of in vivo studies were further verified by in vitro autoradiography in the same animals.

## MATERIALS AND METHODS

### Animals

Fifteen male Sprague–Dawley rats ( $502 \pm 46$  g) were housed in a 12-h light/dark cycle at 22°C with access to food and water ad libitum. All experiments were approved by the German regional authorities (Das Landesamt für Natur, Umwelt, und Verbraucherschutz) and conducted according to the German Animal Welfare Act.

Received Oct. 16, 2012; revision accepted Feb. 12, 2013.

For correspondence or reprints contact: David Elmenhorst, Institute of Neuroscience and Medicine (INM-2), Forschungszentrum Jülich, 52425 Jülich, Germany.

E-mail: d.elmenhorst@fz-juelich.de

Published online Jun. 5, 2013.

COPYRIGHT © 2013 by the Society of Nuclear Medicine and Molecular Imaging, Inc.

In all animals, respiration rate (pressure pad), heart rate (electrocardiogram), and body temperature (rectal probe) were monitored throughout the scans (BioVet System; m2m Imaging). A heating pad attached to the scanner bed was automatically regulated on the basis of feedback data from the body temperature.

In all animals, arterial blood samples were drawn and input data were corrected for metabolites. The ligand was injected either as a bolus ( $n = 5$ ) or as a bolus plus constant infusion ( $n = 10$ ). Five animals of the latter group received additionally the antagonist 8-cyclopentyl-1,3-dipropylxanthine (DPCPX) during the steady-state phase of ligand delivery. The brains of those animals that did not receive DPCPX were subsequently removed and used for saturation binding using high-resolution *in vitro* autoradiography.

### Arterial Blood Sampling, Tracer Application, and Metabolite Correction

For blood collection, a polyethylene tube (PE50; Becton-Dickinson) (catheter length, 12 cm; dead volume, 30  $\mu$ L) was inserted into the femoral artery under general anesthesia (1.8% isoflurane at an oxygen

flow of 1 l/min). Another catheter was placed either in the femoral vein ( $n = 2$ ) or in the tail vein ( $n = 13$ ) and served for tracer application. A syringe pump (model 44; Harvard Apparatus) was used to infuse either 1 mL of radiotracer over 1 min for the bolus experiments or 2 mL over 2 h for the bolus-plus-constant-infusion experiments, respectively. In bolus-plus-constant-infusion experiments, the fractions of bolus and constant infusion were applied over 1 and 119 min, respectively. Three different bolus-infusion ratios ( $k_{\text{Boi}}$ ) were tested according to simulations based on data from the bolus experiments: 76 min ( $n = 1$ ), 65 min ( $n = 1$ ), and 48 min ( $n = 8$ ).

Blood samples were collected every 10 s for the first 3 min; then at 5, 7, and 10 min; then every 10 min until 90 min; and finally at 105 and 120 min. To prevent hypovolemia, the dead volume was collected in syringes prefilled with 50  $\mu$ L of heparin solution (20 international units/mL) and reperused after each blood collection. Coagulation inside the catheter was prevented by flushing with heparinized saline solution after sampling. All whole-blood and plasma samples were weighed and measured in a high-sensitivity  $\gamma$ -counter (ISOMED 2100; Medizintechnik Dresden) to calculate the activity concentration. Targeted volumes of whole-blood samples were less than 10  $\mu$ L for the first 3 min and less than 100  $\mu$ L per sample thereafter, for a total of  $3.2 \pm 0.4$  mL per experiment.

The sample at 1 min and all samples after 3 min (except 7 min) were used for metabolite determination. Individual fractions of free tracer in plasma (i.e., unbound to plasma proteins; denoted by  $f_p$ ) were assessed by ultrafiltration after incubating whole-blood samples with  $^{18}\text{F}$ -CPFPX (5).

The activity concentrations of whole blood and plasma (centrifugation of whole blood for 3 min at 3,000g) were quantified. The fraction of intact radioligand in total plasma activity was determined as previously described (7) with slight modifications of the amount of extraction solvent (350  $\mu$ L) and duration of centrifugation (5 min).

### PET Acquisition, Reconstruction, and Image Analysis

PET measurements were performed on an Inveon scanner (Siemens). The animals lay supine with their heads immobilized by both the body holder and the nose cone of the anesthesia delivery (1.8% isoflurane at an oxygen flow of 1 L/min). A 10-min dual-source  $^{57}\text{Co}$  transmission scan was acquired to correct for attenuation. In 2 animals, a CT-based attenuation correction map was used.

List-mode PET data were acquired for 120 min after tracer injection and framed into a dynamic sequence of  $12 \times 10$ -s,  $3 \times 20$ -s,  $3 \times 30$ -s,  $3 \times 60$ -s,  $3 \times 150$ -s,  $13 \times 300$ -s, and  $4 \times 600$ -s frames. One hundred fifty-nine slices of 0.796-mm thickness (pixel size,  $0.7764 \times 0.7764$  mm; 128 pixels) were reconstructed by filtered backprojection (ramp filter; cutoff, 0.5) after Fourier rebinning into 2-dimensional sinograms (corrected for random coincidences, scatter radiation, and attenuation).

Four animals were additionally scanned using CT (Inveon), and CT planes were

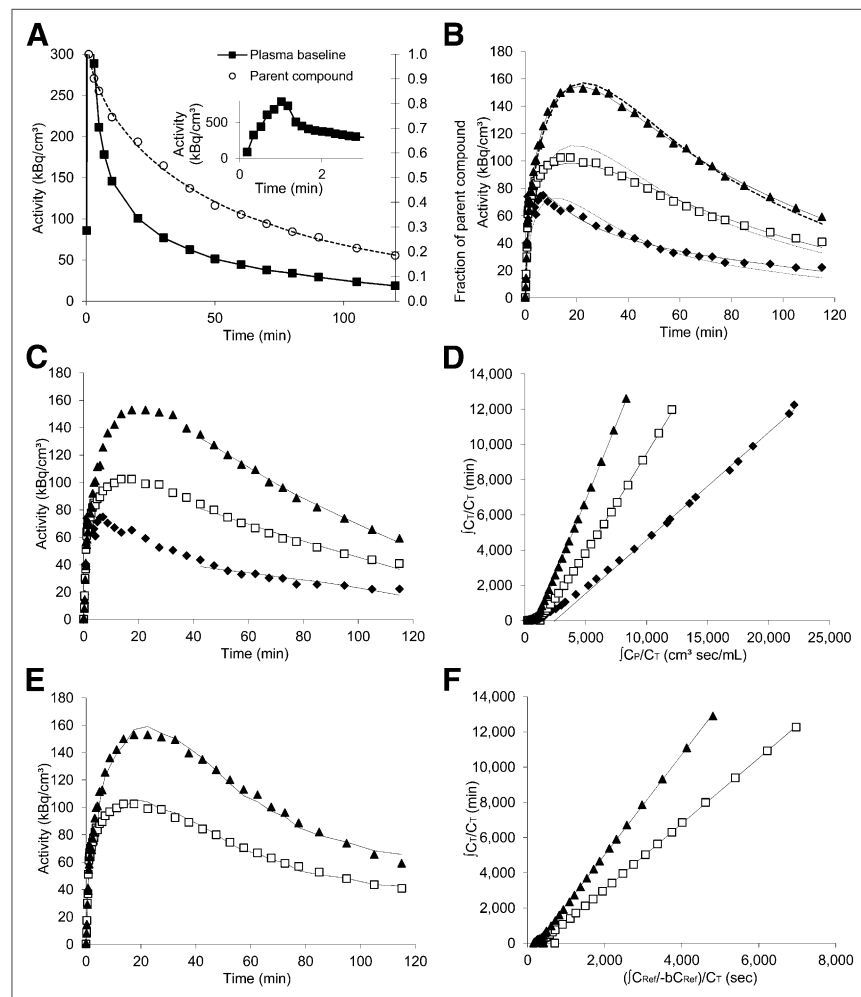


**FIGURE 1.** Kinetics of bolus injection time-activity curves of plasma (A) and tissue (B, C, and E), graphical analysis plots (D and F) and fits in selected regions of interest (◆ = olfactory bulb region; □ = cortex region; ▲ = thalamus region) of representative control rat. (A) Plasma activity (■, left y-axis) and fraction of intact ligand (○, right y-axis) of same rat. Inset shows plasma peak in first minutes. Plasma activities are normalized to injected dose and body weight. (B) Fits of 1TCM (dashed line) and 2TCM (straight line). (C) MA1 with arterial input function. (D) Graphical analysis with arterial input function. (E) Fits based on SRTM. (F) Graphical analysis using reference region input.

**TABLE 1**  
 Bolus Injection: In Vivo Binding Parameters Obtained with Metabolite-Corrected Plasma Input Function

Region	$V_T$ (mL/cm <sup>3</sup> )			
	1TCM	2TCM	MA1	GA
Olfactory bulb	0.54 ± 0.10 (18%)	0.64 ± 0.11 (17%)	0.66 ± 0.11 (16%)	0.66 ± 0.10 (15%)
Caudate-putamen	1.60 ± 0.38 (24%)	1.69 ± 0.37 (22%)	1.64 ± 0.34 (21%)	1.63 ± 0.33 (20%)
Cerebellum gray matter	1.59 ± 0.37 (23%)	1.66 ± 0.33 (20%)	1.64 ± 0.33 (20%)	1.64 ± 0.31 (19%)
Cortex	1.17 ± 0.22 (19%)	1.24 ± 0.22 (18%)	1.24 ± 0.21 (17%)	1.24 ± 0.18 (15%)
Hippocampus	1.71 ± 0.39 (23%)	1.80 ± 0.36 (20%)	1.76 ± 0.35 (20%)	1.76 ± 0.34 (19%)

GA = graphical analysis.

$n = 5$  (±SD and coefficient of variation in %).

manually coregistered with integrated PET images (integrated from 0 to 70 min).

CT images were then manually coregistered with a rat template atlas (PMOD, version 3.3; PMOD Group). The 4 integrated PET images were averaged and used as a template for the remaining scans. First, integrated PET images were coregistered manually to the PET template, and second, the automatic coregister tool from SPM5 (Wellcome Trust Centre for Neuroimaging) was used. After a check for potential head movements using a video consisting of the PET frames, the transformation matrix was applied to each frame.

Regional time-activity curves based on volumes of interest defined on the rat template were calculated for the following brain regions: cerebral cortex (mean total volume of left and right hemisphere, 0.59 cm<sup>3</sup>), cortex without entorhinal cortex (0.51 cm<sup>3</sup>), cingulate cortex (0.03 cm<sup>3</sup>), entorhinal cortex (0.12 cm<sup>3</sup>), pons (0.05 cm<sup>3</sup>), medulla oblongata (0.06 cm<sup>3</sup>), thalamus (0.06 cm<sup>3</sup>), hypothalamus (0.04 cm<sup>3</sup>), nucleus accumbens (0.02 cm<sup>3</sup>), olfactory bulb (0.05 cm<sup>3</sup>), hippocampus (0.07 cm<sup>3</sup>), caudate-putamen (0.09 cm<sup>3</sup>), and cerebellum (0.15 cm<sup>3</sup>). The defined regions covered all anatomic structures of interest.

### Kinetic Models

Ligand binding is dependent on the amount of available receptors ( $B_{avail}$ ) and the affinity of the ligand for the receptor ( $1/K_D$ ). Practically, parameters that are related to this product (binding potential) can be determined in various ways (8). One substitute is the total distribution volume ( $V_T$ ), which is the concentration of the radioligand

in the brain region related to the concentration of the radioligand in plasma at equilibrium. The equilibrium  $V_T$  is composed of a specific distribution volume ( $V_S$ , equal to  $f_P B_{avail}/K_D$ ), with  $f_P$  being the fraction of free ligand in plasma and the distribution volume of free and nonspecifically bound ligand ( $V_{ND}$ ).  $V_T$  was determined by the following models: standard 1- and 2-tissue-compartment models (1TCM and 2TCM, respectively), Logan graphical analysis, and multilinear analysis (MA1). For the bolus-plus-constant-infusion experiments,  $V_T$  was determined by the tissue-to-plasma ratio during the steady-state phase (50–70 min). For kinetic analyses, only data up to 70 min were used (to allow inclusion of DPCPX competition studies).

Regional binding potentials related to the nondisplaceable uptake ( $BP_{ND}$ ) as a second measure of ligand binding (8) were determined by the following kinetic models based on the olfactory bulb time-activity curve as input: simplified reference tissue models (SRTM/SRTM2), Logan noninvasive graphical analysis, multilinear reference tissue model, and the ratio of distribution volumes from the  $V_T$  of the 2TCM in target and reference region. Parametric images were generated representing  $BP_{ND}$  by the SRTM2 model. A more detailed description of the kinetic models can be found in the supplemental material (available online at <http://jnm.snmjournals.org>).

Scanning times were artificially shortened by iteratively omitting the last PET frames to test to what extent kinetic models depend on scan duration. Data were in each case remodeled and normalized to the 120-min value.

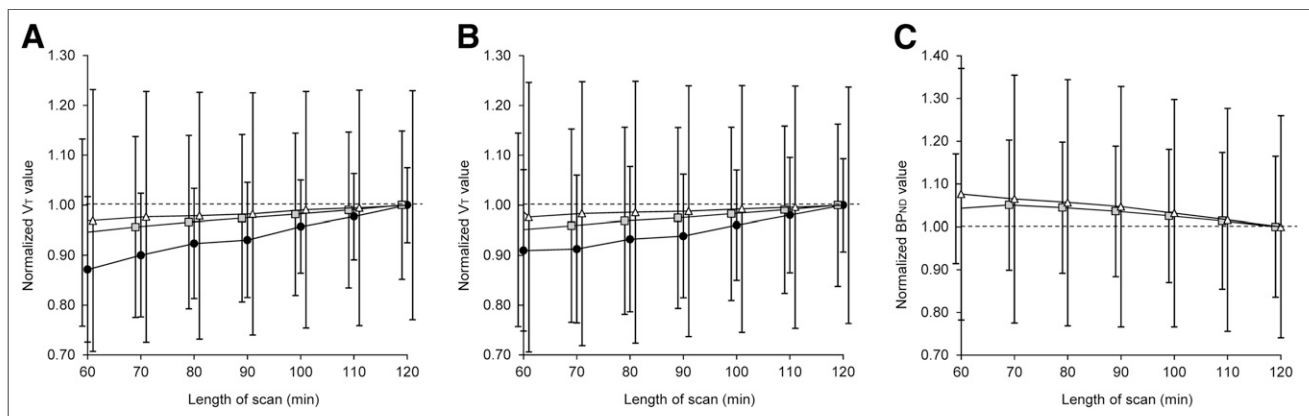


**FIGURE 2.** Time stability of  $V_T$  determination of bolus injection experiments using 2TCM (A) and MA1 (B) and of  $BP_{ND}$  using SRTM (C). y-axis represents actual outcome parameter determined after artificial shortening of scan time (x-axis) divided by respective outcome parameter with full scan length. Error bars represent coefficient of variation (SD divided by each  $V_T/BP_{ND}$  value of respective scan duration) ( $n = 5$ ). ● = olfactory bulb region; □ = cortex region; △ = thalamus region.

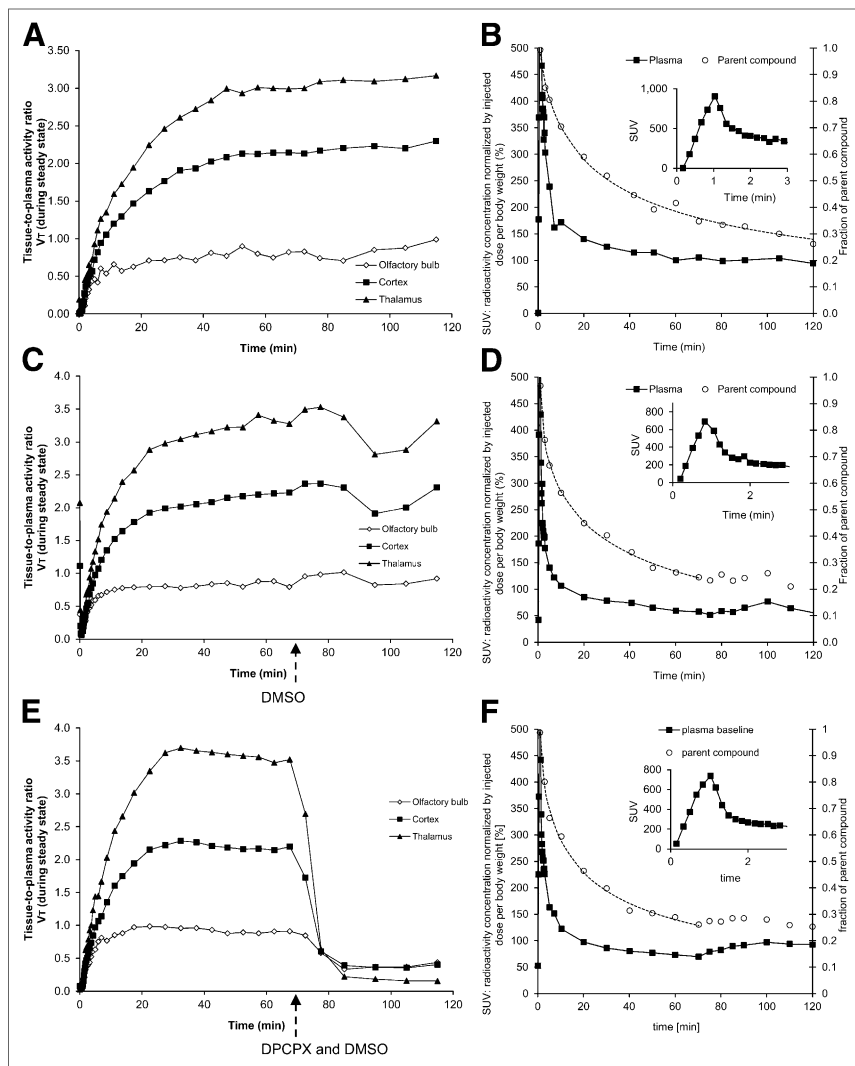


**FIGURE 3.** Tissue plasma ratios representing total distribution volume (A, C, and E) of bolus-plus-constant-infusion scheme in selected regions of interest ( $\diamond$  = olfactory bulb region;  $\blacksquare$  = cortex region;  $\blacktriangle$  = thalamus region) and respective plasma activity of parent compound and fraction of metabolites (B, D, and F). A and B show control, C and D show vehicle, and E and F show displacement experiment. Vehicle dimethylsulfoxide and displacer DPCPX (in dimethylsulfoxide) were administered after 70 min as indicated by arrows. Plasma activity ( $\blacksquare$ , left y-axis) and fraction of intact ligand ( $\circ$ , right y-axis) are shown. Inset shows plasma peak in first minutes. Plasma activities are normalized to injected dose and body weight.

### Blocking Experiments

Specific binding was blocked during a bolus-plus-constant-infusion scan by the antagonist DPCPX to evaluate the olfactory bulb as a reference region. DPCPX was administered by slow intravenous infusion at 70 min with a dose of 0.5 mg in 80  $\mu$ L ( $n = 3$ ) and 300  $\mu$ L ( $n = 2$ ) of dimethylsulfoxide. One animal received only the vehicle (300  $\mu$ L of dimethylsulfoxide). We observed a transient acceleration of the respiration rate and a slight hemolysis after 20–30 min.

### Radioligands and Chemicals

$^3$ H-DPCPX (specific activity, 4,440 GBq/mmol) was purchased from PerkinElmer. All other chemicals were of reagent grade and obtained commercially.  $^{18}$ F-CPFPX was synthesized as described previously (9).

At the start of the scan, the mean specific radioactivity was  $127 \pm 137$  GBq/ $\mu$ mol. Mean injected radioactivity was  $21.3 \pm 8.5$  MBq. The

mass of injected CPFPX per body weight was  $1.2 \pm 1.3$  nmol/kg. The  $f_p$  value was on average  $2.0\% \pm 1.1\%$ .

A detailed description of the autoradiographic experiments can be found in the supplemental “Material and Methods.”

All reported average values are mean  $\pm$  SD.

## RESULTS

The pharmacokinetic properties of  $^{18}$ F-CPFPX were investigated separately for the bolus and the bolus-plus-constant-infusion experiments with both arterial and reference input functions.

### Bolus Injection Experiments: Input Function and Kinetic Analyses

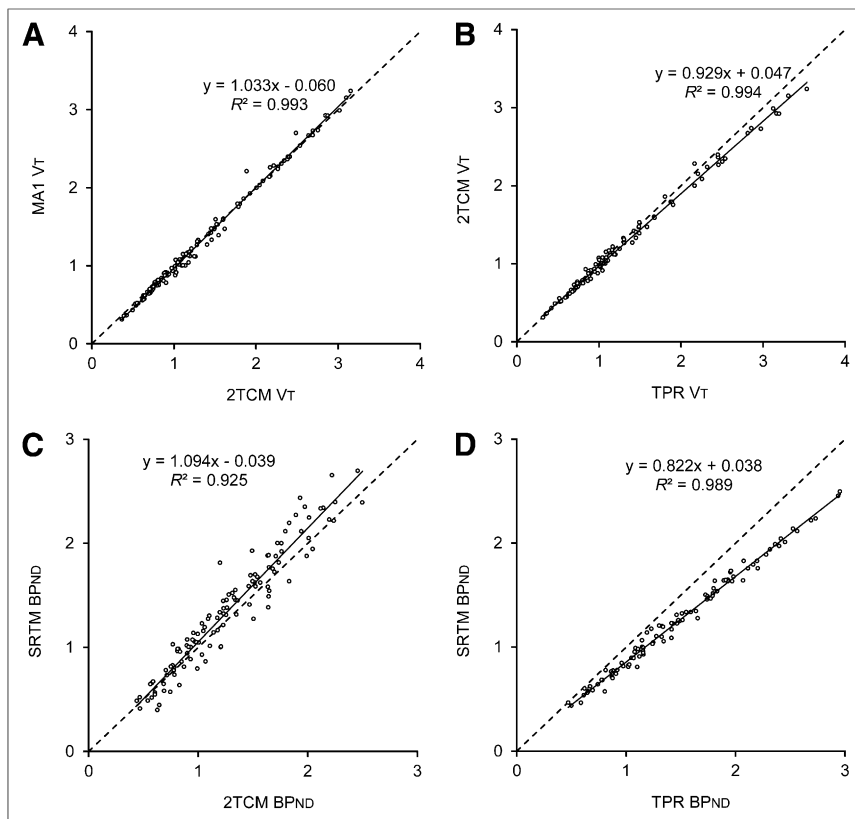
The time course of the plasma concentration of the intact ligand and the degree of metabolism are shown in Figure 1A. During the 1-min injection, ligand concentrations increased in plasma and tissue nearly linearly and decreased rapidly thereafter. Although no metabolism of  $^{18}$ F-CPFPX was observed in the 1-min sample, 50% of the compound was metabolized after about 35 min. The ratio of plasma to whole-blood activity was between 1.5 and 1.7. The extraction fraction from the plasma protein precipitation was virtually constant, with  $98\% \pm 1\%$  extraction after 120 min.

Figure 1B shows representative time–activity curves for the olfactory bulb, cortex, and thalamus. Radioactivity concentration peaked after 5 min in the low-binding region (olfactory bulb) and at 23 min in the high-binding region (thalamus) and decreased thereafter. Tissue-to-plasma ratio increased but did not peak during scanning, reaching 90% of the 120-min value at around 60 min. Tissue-to-olfactory bulb ratio peaked at between 30 and 45 min.

The 2TCM was superior to the 1TCM as proved by significantly lower values of the Akaike information criteria. The  $V_T$  based on the 2TCM was highest in the thalamus ( $1.8$  mL/cm $^3$ ) and lowest in the olfactory bulb ( $0.6$  mL/cm $^3$ ). There was no correlation between injected dose and  $V_T$ . Graphical analysis and MA1 revealed  $V_T$  estimates that were in excellent agreement with the 2TCM  $V_T$  ( $R^2 = 0.99$ ): the correlation graphs are provided in Supplemental Fig. 1). Average  $V_T$  values for selected regions and models are presented in Table 1.

### Reference Tissue-Based Kinetic Analyses

The olfactory bulb was chosen as the reference region for testing noninvasive quantification. Although the 1TCM did not describe olfactory bulb kinetics adequately, the 2TCM did so. Comparison of SRTM  $BP_{ND}$  and the  $BP_{ND}$  based on the 2TCM revealed an average bias of  $4.4\% \pm 13\%$  in the cortex and a bias of  $5.3\% \pm 10\%$  in the high-binding region thalamus (Table 2 and correlation sketch: Supplemental Fig. 1B). Such a bias has already



**FIGURE 4.** Bolus infusion experiments: correlations of distribution volume ( $V_T$ ) and  $BP_{ND}$  derived by different nonlinear, linear, multilinear, and equilibrium methods (data from 0 to 70 min). (A) Correlation between  $V_T$  of 2TCM and MA1. (B) Correlation between  $V_T$  of 2TCM and tissue-to-plasma ratio (TPR) during steady-state phase. (C) Correlation between  $BP_{ND}$  derived from  $V_T$  of 2TCM and SRTM. (D) Correlation between  $BP_{ND}$  based on SRTM and tissue-to-plasma ratio during steady-state phase. Solid line represents linear regression analysis and dotted line identity. Results of regression are depicted for 13 regions ( $n = 10$  except for tissue-to-plasma ratio:  $n = 8$ ).

been reported for other radioligands (10), and the reason might be that the assumptions of the SRTM are violated since both the reference region and the specific binding regions require 2 compartments. The correlations between  $BP_{ND}$  based on the 2TCM and SRTM showed the highest variability ( $R^2 = 0.94$ ) among the correlations performed for this study. When the data of only one animal at a time are correlated, the variability is lower, with coefficients being higher than 0.97. Differences in model accordance between animals explain part of the overall variability of this comparison. Excellent correlation without noticeable bias was found within the reference model itself (Supplemental Fig. 1D).

Time stability was evaluated for the bolus experiments ( $n = 5$ ). 2TCM, MA1, and SRTM yielded stable outcome parameters in terms of bias and variance for acquisition times of 70 min (Fig. 2). Especially for MA1 and SRTM, the bias was less than 6%, compared with a 120-min scan duration in higher-binding regions (cortex and thalamus). Shortening the scan length increased the coefficient of variation slightly (Fig. 2); for example, in the cortex, the coefficient of variation increased from 17% at 120 min to 18% at 70 min for MA1 and from 15% to 18%, respectively, for 2TCM. Scanning time is a tradeoff between experimental effort and animal strain due to anesthesia (which has to be minimized) and the noise, bias, and increased variability of the outcome parameters that are introduced because of the restricted amount of data. As

a compromise, 70 min of dynamic data on  $^{18}\text{F}$ -CPFPX binding is considered suitable for the quantitative assessment of cerebral  $A_1$ ARs. This conclusion has to be reevaluated in the presence of pharmaceuticals that affect binding or metabolism of  $^{18}\text{F}$ -CPFPX.

### Bolus-Plus-Constant-Infusion Experiments: Kinetic and Equilibrium Analyses

For kinetic analyses, the first 70 min were used to compare compartment, reference, and equilibrium methods. Bolus-infusion ratios of 76 and 65 min did not lead to a steady-state condition in plasma or brain tissue. A further reduction of  $k_{\text{Bol}}$  to 48 min established slightly decreasing activity concentrations indicated by a mean rate of change between 50 and 70 min of  $-17.4\% \pm 21\%/h$  in plasma,  $-0.8\% \pm 29\%/h$  in the olfactory bulb, and  $-19.9\% \pm 16\%/h$  in the thalamus ( $n = 8$ ). Figures 3A and 3B show the tissue-to-plasma ratio of different regions of interest and the time course of plasma and metabolites for a single rat. The matches of the  $V_T$  and  $BP_{ND}$  values determined by various models and the tissue-to-plasma ratio are depicted in Figure 4. Respective mean values for selected regions and models are presented in Tables 3 and 4. There was good agreement among the distribution volumes and a moderate bias between equilibrium and kinetic reference methods.

### Displacement of Binding

Displacing  $^{18}\text{F}$ -CPFPX with DPCPX resulted in an average decrease of  $V_T$  between 46% and 96% (olfactory bulb and thalamus, respectively) as determined with tissue-to-plasma ratio. A representative example is given in Figures 3E and 3F. The olfactory bulb time-activity curve decreased on average by 29% 30 min after the start of displacement, whereas the plasma activity increased at the same time by on average 28%. Both changes together led to the observed reduction in the olfactory bulb  $V_T$ . Figures 3C and 3D show that 300  $\mu\text{L}$  of the vehicle dimethylsulfoxide led to a transient increase of  $^{18}\text{F}$ -CPFPX plasma concentration 30 min after injection. Tissue activity concentration peaked 5–10 min later than plasma concentration, leading to a transient decrease in the tissue-to-plasma ratios of approximately 15% until steady state was reestablished. Occupancy was determined by the Lassen plot, where  $V_T$  baseline is plotted versus  $V_T$  baseline –  $V_T$  displacement (Supplemental Fig. 2A). The correlation should be linear, and the intercept with the  $x$ -axis gives an approximation of the  $V_{ND}$  and the slope of the line the occupancy level (11). This method revealed a blockade of about  $114\% \pm 30\%$  and a  $V_{ND}$  of 0.29  $\text{mL}/\text{cm}^3$ .  $A_1$ AR occupancy by DPCPX was higher than 100%. This overestimation is in line with the observation that displacement in the high-binding regions (thalamus and hippocampus) led to lower activity concentrations than did displacement in the low-binding region (olfactory bulb). An occupancy plot without olfactory bulb, thalamus,

**TABLE 2**  
In Vivo Binding Parameters Obtained with Reference Tissue Input Function After Bolus Injection

Region	$BP_{ND}$				
	SRTM	MRTM	2TCM	MA1	NIGA
Caudate–putamen	1.69 ± 0.28 (16%)	1.72 ± 0.23 (14%)	1.64 ± 0.33 (20%)	1.46 ± 0.27 (19%)	1.47 ± 0.26 (17%)
Cerebellum gray matter	1.67 ± 0.23 (14%)	1.68 ± 0.22 (13%)	1.6 ± 0.33 (20%)	1.47 ± 0.26 (18%)	1.49 ± 0.25 (17%)
Cortex	1 ± 0.1 (10%)	1 ± 0.08 (8%)	0.94 ± 0.06 (7%)	0.86 ± 0.05 (6%)	0.88 ± 0.04 (4%)
Hippocampus	1.8 ± 0.26 (14%)	1.84 ± 0.24 (13%)	1.82 ± 0.34 (18%)	1.65 ± 0.29 (18%)	1.67 ± 0.27 (16%)

MRTM = multilinear reference tissue model; NIGA = noninvasive graphical analysis.  
 $n = 5$  ( $\pm$ SD and coefficient of variation in %).

and hippocampus showed  $93\% \pm 6\%$  occupancy and a  $V_{ND}$  of  $0.12 \text{ mL/cm}^3$  (Supplemental Fig. 2B). Figure 5A shows the activity distribution in a sagittal section of the brain and skull during the baseline period and after displacement with DPCPX (PET with CT overlay). Spillover of activity from parts of the brain more posterior to the olfactory bulb is observed in the baseline condition. After displacement, we find a different situation, with a spillover of activity from the surrounding tissue into the olfactory bulb. This effect is especially aggravated in later scanning periods, when a higher fraction of radioactive metabolites, which do not cross the blood–brain barrier, exists in the blood. Thus, the specific anatomic localizations of the investigated structures (olfactory bulb close to blood-rich structures vs. thalamus and hippocampus distant from the brain surface) will contribute to the seemingly lower displacement in the olfactory bulb than in the thalamus and hippocampus.

#### Parametric Images

The typical distribution of  $A_1AR$  in the rat brain is in good accordance with the distribution pattern on autoradiography (Fig. 5).

Average parametric images ( $n = 14$ ) of  $BP_{ND}$  calculated by application of the SRTM2 are presented in Figure 6. Parametric images based on noninvasive graphical analysis or the multilinear reference tissue model showed considerable noise and several voxels where the modeling failed. In contrast, SRTM2 could be successfully applied in all animals. An excellent congruency without noticeable bias ( $0.15\%$  in pons and  $-0.6\%$  in thalamus) to the region-of-interest time–activity curve–based SRTM analysis (regression,  $y = 0.991x + 0.027$ ;  $R^2 = 0.98$ ;  $P < 0.0001$ ) was ob-

served when the same region of interest as for time–activity curve generation was overlaid on the parametric images.

#### Autoradiography and Saturation Binding

$^3H$ -DPCPX binding to rat brain slices was saturable and displaceable. It was well described by the single-site binding model, which revealed  $B_{max}$  values between 30 and 530 fmol/mg (tissue) (medulla oblongata and cerebellum, across animals, respectively) and  $K_D$  values between 0.16 and 0.98 nM (across animals)—on average 0.45 nM. A representative section of total and nonspecific binding is depicted in Figure 5B. The use of a single-site binding model was confirmed by the near-identity slope of the Hill plot (on average,  $0.97 \pm 0.04$ ).

In vivo PET and in vitro autoradiographic measures in the same animals ( $n = 9$ ) showed a significant linear correlation. Figure 7 displays the correlations of  $V_T$  and  $B_{max}$  (Pearson correlation,  $P < 0.0001$ ; regression data provided in the figure) and of  $BP_{ND}$  and  $B_{max}$  ( $P < 0.0001$ ). Specific binding was found in the in vitro data for the olfactory bulb ( $\sim 100 \text{ fmol/mg}$  [tissue]).

#### DISCUSSION

In the present study, we compared in vivo and in vitro determinations of the cerebral  $A_1AR$  in subsequent investigations of the same animals. By this means, pharmacokinetic models for the quantification of the PET radiotracer  $^{18}F$ -CPFPX were evaluated on the basis of metabolite-corrected plasma input function and a reference tissue approach.

The primary objective was to verify whether reference tissue methods are suitable to provide measures of rat brain  $A_1AR$ . We

**TABLE 3**  
Bolus-and-Infusion Equilibrium Measurement: In Vivo Binding Parameters Obtained with Metabolite-Corrected Plasma Input Function in 5 Brain Regions

Region	$V_T$ ( $\text{mL/cm}^3$ )				
	1TCM	2TCM	MA1	GA	TPR
Olfactory bulb	0.5 ± 0.23 (46%)	0.54 ± 0.24 (44%)	0.59 ± 0.24 (41%)	0.57 ± 0.23 (41%)	0.52 ± 0.22 (43%)
Caudate–putamen	1.54 ± 0.78 (51%)	1.57 ± 0.79 (50%)	1.57 ± 0.77 (49%)	1.55 ± 0.75 (49%)	1.63 ± 0.87 (53%)
Cerebellum gray matter	1.47 ± 0.74 (50%)	1.5 ± 0.76 (51%)	1.52 ± 0.74 (49%)	1.51 ± 0.73 (48%)	1.56 ± 0.84 (54%)
Cortex	1.11 ± 0.57 (51%)	1.14 ± 0.59 (52%)	1.18 ± 0.58 (49%)	1.17 ± 0.56 (48%)	1.18 ± 0.64 (54%)
Hippocampus	1.62 ± 0.8 (49%)	1.64 ± 0.83 (50%)	1.67 ± 0.81 (48%)	1.65 ± 0.78 (47%)	1.72 ± 0.9 (52%)

GA = graphical analysis; TPR = tissue-to-plasma ratio.  
 $n = 8$  ( $\pm$ SD and coefficient of variation in %).

TABLE 4

Bolus-and-Infusion Equilibrium Measurement: In Vivo Binding Parameters Obtained with Reference Tissue Input Function

Region	$BP_{ND}$					
	2TCM	MA1	NIGA	TPR	MRTM	SRTM
Caudate-putamen	1.88 ± 0.32 (17%)	1.59 ± 0.28 (17%)	1.7 ± 0.27 (16%)	2.04 ± 0.31 (15%)	1.71 ± 0.27 (16%)	1.73 ± 0.25 (15%)
Cerebellum gray matter	1.73 ± 0.25 (15%)	1.51 ± 0.24 (16%)	1.62 ± 0.26 (16%)	1.91 ± 0.29 (15%)	1.62 ± 0.24 (15%)	1.65 ± 0.23 (14%)
Cortex	1.07 ± 0.2 (19%)	0.94 ± 0.16 (17%)	1.02 ± 0.14 (14%)	1.19 ± 0.24 (20%)	1 ± 0.18 (18%)	1.01 ± 0.18 (18%)
Hippocampus	2 ± 0.29 (14%)	1.77 ± 0.25 (14%)	1.87 ± 0.23 (13%)	2.21 ± 0.3 (13%)	1.85 ± 0.23 (13%)	1.84 ± 0.23 (12%)

NIGA = noninvasive graphical analysis; TPR = tissue-to-plasma ratio; MRTM = multilinear reference tissue model.  
 $n = 8$  ( $\pm$ SD and coefficient of variation in %).

conclude that the olfactory bulb can be used as a reference region for noninvasive quantification because of the following findings. First, the outcome of arterial input function-based parameters correlates with a low bias to reference region-based input quantification (correlation of 2TCM  $BP_{ND}$  to SRTM  $BP_{ND}$ ). Second, autoradiographic receptor estimations correlated with PET quantification ( $B_{max}$  vs.  $BP_{ND}$ ). Third, nearly complete blockade of binding had the lowest effect of all investigated regions on olfactory bulb  $V_T$ . Fourth, the level of nondisplaceable uptake in the reference region and the region of interest is the same as shown by the linearity of the Lassen plot of occupancy. The olfactory bulb is therefore considered a suitable reference region for noninvasive quantification of  $^{18}F$ -CPFPX PET data as long as the specific binding in this region is kept in mind.

The use of the reference region approach will substantially ease future  $^{18}F$ -CPFPX PET studies, allowing minimally invasive longitudinal and repetitive measurements in the same animals.

Modeling cerebral  $^{18}F$ -CPFPX distribution with a 2TCM described the time-activity curves adequately and correlated well with noncompartmental models such as graphical analysis and MA1. Stable fitting results for the MA1 method were achieved when scanning times of at least 70 min were used.

A correction of  $f_p$  was not included because it increased noise rather than reducing it.

There was a bias between SRTM  $BP_{ND}$  and 2TCM  $BP_{ND}$  due to nonunity of correlations. It was most pronounced in a high-binding region (hippocampus), with an average bias of 13%. However, the relationships were linear and provided an adequate estimate of receptor density as evidenced by the linear correlation with data from in vitro autoradiography. Similar phenomena have already been observed for other PET radioligands (12,13).

We suggest that the MA1 model should be preferred when an arterial input function is used to calculate  $V_T$ , whereas SRTM is the model of choice for noninvasive determinations of  $BP_{ND}$ .

To achieve equilibrium in bolus-plus-constant-infusion experiments, we tested different  $k_{B0l}$  values and found increasing activity concentrations with a  $k_{B0l}$  of 48 min whereas  $k_{B0l}$  times of 76 and 65 min led to decreasing time-activity curve and plasma concentrations. A perfect equilibrium will therefore require a  $k_{B0l}$  of around 58 min. Nevertheless, compared with the values of the 2TCM, the error introduced by an imperfect equilibrium is below 5% (Table 3). The bolus-plus-constant-infusion group had a higher variability in  $V_T$  than did the bolus injection group (coefficient of variation of 15%–24% vs. 41%–54%). When looking at the interindividual differences of the animals, it is evident that the higher SD of the infusion group is caused by 2 animals with higher binding than the other animals (hippocampal  $V_T$  of about 2.9 mL/cm<sup>3</sup>).

A series of blocking experiments revealed that DPCPX is effectively competing with  $^{18}F$ -CPFPX. The  $V_{ND}$  by use of the occupancy plot is lower than the olfactory bulb  $V_T$  (0.48 mL/cm<sup>3</sup>,  $n = 5$ ), which is proposed here as  $V_{ND}$  indicating specific binding in this region.

To evaluate whether the experiments were performed at tracer doses, we used the approach based on  $K_D^{in vivo}$  (calculated from the slope of the correlation of autoradiography and PET (13), as described below), peak uptake value in the reference region, and fraction of free and nondisplaceable tracer in tissue ( $f_{ND} = f_p/V_{ND}$  (8)). Less than 5% occupancy of receptors was considered the limit of the injected dose. The average injected dose was 26 MBq ( $n = 9$ ), and olfactory bulb peak activity was 72 kBq/cm<sup>3</sup>, resulting in a peak uptake fraction of 2.8 l/L reflecting the nondisplaceable concentration. Together with an  $f_{ND}$  of 0.03 and a  $K_D^{in vivo}$  of 3.8 nM, the dose limit was estimated at 2.3 nmol [occupancy =  $F/(F + K_D)$ , with  $F$  = injected

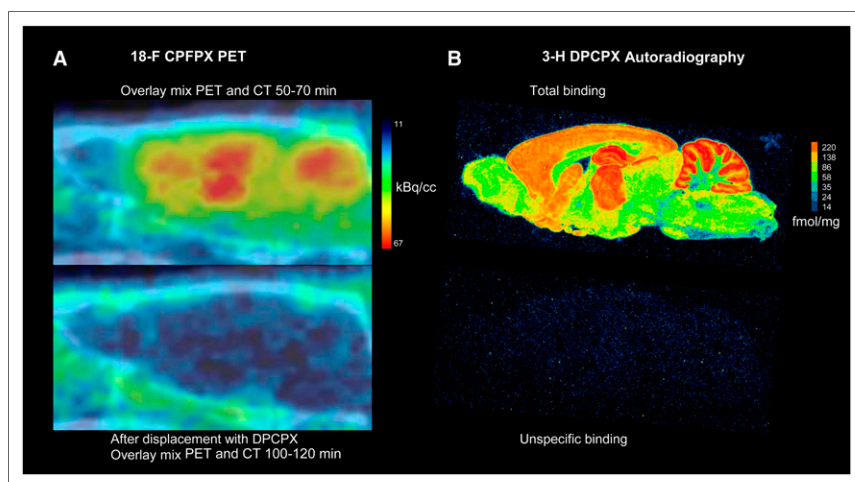


**FIGURE 5.** Effect of blockade of  $A_1AR$  in vivo and in vitro. Sagittal sections of rat brain representing  $A_1AR$  distribution and nonspecific binding at level of caudate-putamen and hippocampus as detected by PET (A) and autoradiography (B). Rat brain autoradiogram (at 1 nM concentration of  $^3H$ -DPCPX) shows receptor total binding and nonspecific binding in presence of R-phenyl-isopropyl-adenosine in 2 adjacent sections.

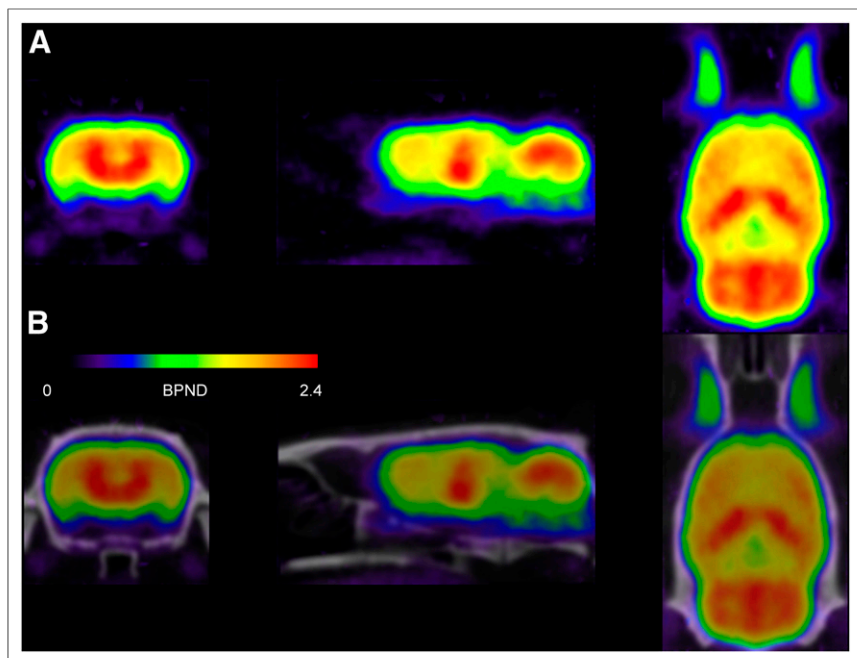


**FIGURE 6.** Coronal, sagittal, and horizontal sections displaying parametric images of  $BP_{ND}$  generated by voxelwise application of SRTM2. Shown are average images of 14 control rats coregistered to rat brain template: without overlay of representative CT image (A) and with overlay (B).

dose  $\times$  uptake fraction  $\times f_{ND}$ . The highest dose injected in this study was 1.9 nmol (average,  $0.61 \pm 0.64$  nmol).

The present study confirms previous reports about the distribution pattern of  $^{18}F$ -CPFPX and  $^3H$ -DPCPX in rats (14). High binding was found in the hippocampus, intermediate binding in the cortex, and low binding in the olfactory bulb and pons.

Binding data from PET and autoradiography were significantly correlated, and most regions of interest were close to the regression line.

$BP_{ND}$  data were in general less variable than  $V_T$  estimates and correlated better with the autoradiography.

In autoradiographic saturation experiments, specific binding was detectable in the olfactory bulb ( $\sim 100$  fmol/mg [tissue]).  $B_{max}$

was small in comparison to the high-binding regions ( $\sim 450$  fmol/mg [tissue]). The ratio of the thalamus to the olfactory bulb is about 5-fold in this assay. When the in vitro finding is translated to the PET setting, where washing steps are not possible and a high amount of nondisplaceable binding is present, the fraction of specific binding in the olfactory bulb can be estimated on the basis of the following assumptions: for the olfactory bulb,  $V_{ND} + V_S = 0.65$  mL/cm<sup>3</sup>, and as  $V_S$  is 5 times higher in the thalamus:  $V_{ND} + 5V_S = 1.85$  mL/cm<sup>3</sup> (graphical analysis). When these equations are combined,  $V_S$  equals 0.3 mL/cm<sup>3</sup>, which is about 45% of the  $V_T$  of the olfactory bulb (assuming that  $V_{ND}$  is homogeneous).

The relation of  $V_T$  and  $BP_{ND}$  versus the in vitro  $B_{max}$  (Fig. 7) offers the possibility to approximate an in vivo  $K_D$  (named  $K_D^{in vivo}$ ): the intercept of  $V_T$  versus  $B_{max}$  is by definition  $V_{ND}$ , and the slope is  $f_P$  over  $K_D^{in vivo}$  times a partial-volume effect factor. The intercept with 0.77 mL/cm<sup>3</sup> is close to the graphical analysis  $V_T$  of 0.65 mL/cm<sup>3</sup> (olfactory bulb without displacement). With the measured  $f_P$  of 0.02 and the slope of 0.0029 1/nM,  $K_D^{in vivo}$  is 6.8

nM times the partial-volume effect factor. Filtering the caudate putamen region from the atlas by a 2-mm gaussian kernel results in a partial-volume effect factor of 0.55. Applying this factor gives a  $K_D^{in vivo}$  of 3.8 nM.

For the  $BP_{ND}$  versus  $B_{max}$  plot, the slope is the free fraction of ligand in the nondisplaceable tissue compartment ( $f_{ND}$ ) over  $K_D^{in vivo}$  times the same partial-volume effect factor and the intercept should be zero. The fit of Figure 7 was close to zero with an intercept of 0.25. Forcing the fit through zero gives a slope of 0.0049 1/nM. Based on these values,  $K_D^{in vivo}$  is 3.4 nM.

Previously, we have carefully evaluated how changes in specific binding in the reference region affect noninvasive outcome parameters such as  $BP_{ND}$  (5). It is important to keep this relation in mind and select applications accordingly when using the olfactory bulb as a reference region.

## CONCLUSION

The present study provides evidence that in rodents,  $^{18}F$ -CPFPX PET can be performed quantitatively on the basis of a reference tissue approach in selected applications. The specific binding in the reference region of about 45% needs careful consideration in quantitative studies. This minimally invasive method will considerably facilitate longitudinal studies of physiologic and pathologic conditions in small-animal models.

## DISCLOSURE

The costs of publication of this article were defrayed in part by the payment of page charges.

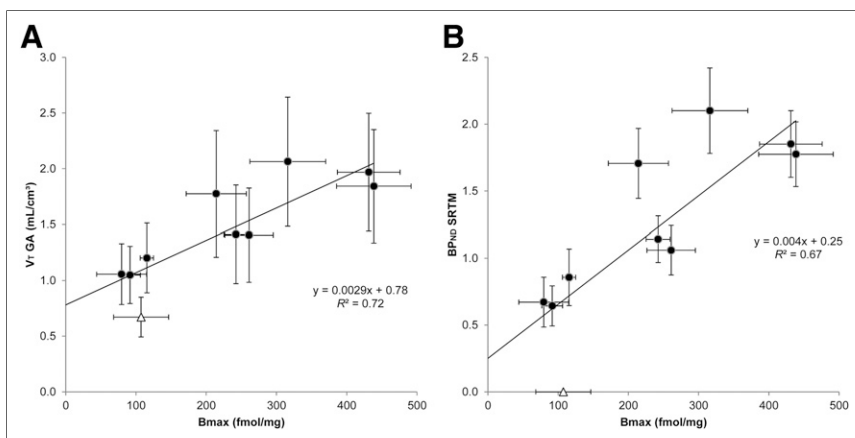


**FIGURE 7.** Comparison of  $A_1AR$  concentrations measured with autoradiographic saturation binding experiments ( $B_{max}$ ) and PET in 10 brain regions. Both total distribution volume  $V_T$  (A) of graphical analysis ( $n = 9$ ) and  $BP_{ND}$  (B) derived from SRTM significantly correlated with  $B_{max}$ . Solid line represents linear regression analysis. Results of regression are given. Error bars denote SD.  $\triangle$  = olfactory bulb.

Therefore, and solely to indicate this fact, this article is hereby marked “advertisement” in accordance with 18 USC section 1734. No potential conflict of interest relevant to this article was reported.

## ACKNOWLEDGMENTS

Magdalene Vögeling, Rishi Gupta, and Nikola Kornadt-Beck are gratefully acknowledged for excellent technical assistance; Claudia Kuntner for providing the software for sampling time logging, and Andreas Matusch for fruitful discussions. Johannes Ermert and Heinz H. Coenen are gratefully acknowledged for radioligand supply.

## REFERENCES

1. Dunwiddie TV, Masino SA. The role and regulation of adenosine in the central nervous system. *Annu Rev Neurosci.* 2001;24:31–55.
2. Paul S, Elsinga PH, Ishiwata K, Dierckx RA, van Waarde A. Adenosine A<sub>1</sub> receptors in the central nervous system: their functions in health and disease, and possible elucidation by PET imaging. *Curr Med Chem.* 2011;18:4820–4835.
3. Porkka-Heiskanen T, Kalinchuk AV. Adenosine, energy metabolism and sleep homeostasis. *Sleep Med Rev.* 2011;15:123–135.
4. Bauer A, Ishiwata K. Adenosine receptor ligands and PET imaging of the CNS. *Handb Exp Pharmacol.* 2009;617–642.
5. Elmenhorst D, Meyer PT, Matusch A, Winz OH, Zilles K, Bauer A. Test-retest stability of cerebral A<sub>1</sub> adenosine receptor quantification using [<sup>18</sup>F]CPFPX and PET. *Eur J Nucl Med Mol Imaging.* 2007;34:1061–1070.
6. Kiesman WF, Elzein E, Zablocki J. A1 adenosine receptor antagonists, agonists, and allosteric enhancers. *Handb Exp Pharmacol.* 2009;25–58.
7. Meyer PT, Bier D, Holschbach MH, et al. Quantification of cerebral A1 adenosine receptors in humans using [<sup>18</sup>F]CPFPX and PET. *J Cereb Blood Flow Metab.* 2004;24:323–333.
8. Innis RB, Cunningham VJ, Delforge J, et al. Consensus nomenclature for in vivo imaging of reversibly binding radioligands. *J Cereb Blood Flow Metab.* 2007;27:1533–1539.
9. Holschbach MH, Olsson RA, Bier D, et al. Synthesis and evaluation of non-carrier-added 8-cyclopentyl-3-(3-[<sup>18</sup>F]fluoropropyl)-1-propylxanthine ([<sup>18</sup>F]CPFPX): a potent and selective A<sub>1</sub>-adenosine receptor antagonist for in vivo imaging. *J Med Chem.* 2002;45:5150–5156.
10. Slifstein M, Parsey RV, Laruelle M. Derivation of [<sup>11</sup>C]WAY-100635 binding parameters with reference tissue models: effect of violations of model assumptions. *Nucl Med Biol.* 2000;27:487–492.
11. Lassen NA, Bartenstein PA, Lammertsma AA, et al. Benzodiazepine receptor quantification in vivo in humans using [<sup>11</sup>C]flumazenil and PET: application of the steady-state principle. *J Cereb Blood Flow Metab.* 1995;15:152–165.
12. Parsey RV, Slifstein M, Hwang DR, et al. Validation and reproducibility of measurement of 5-HT<sub>1A</sub> receptor parameters with [carbonyl-<sup>11</sup>C]WAY-100635 in humans: comparison of arterial and reference tissue input functions. *J Cereb Blood Flow Metab.* 2000;20:1111–1133.
13. Gallezot JD, Nabulsi N, Neumeister A, et al. Kinetic modeling of the serotonin 5-HT<sub>1B</sub> receptor radioligand [<sup>11</sup>C]P943 in humans. *J Cereb Blood Flow Metab.* 2010;30:196–210.
14. Fastbom J, Pazos A, Palacios JM. The distribution of adenosine A1 receptors and 5'-nucleotidase in the brain of some commonly used experimental animals. *Neuroscience.* 1987;22:813–826.